Journal of Controlled Release xxx (2012) xxx–xxx

Contents lists available at SciVerse ScienceDirect

Journal of Controlled Release

journal homepage: www.elsevier.com/locate/jconrel

Mechanism of transport of saquinavir-loaded nanostructured lipid carriers across the intestinal barrier

Ana Beloqui [a,b], María Ángeles Solinís [a], Alicia R. Gascón [a], Ana del Pozo-Rodríguez [a], Anne des Rieux [b,*], Véronique Préat [b,*]

[a] Pharmacokinetics, Nanotechnology and Gene Therapy Group, Laboratory of Pharmacy and Pharmaceutical Technology, School of Pharmacy, University of the Basque Country UPV/EHU, Vitoria-Gasteiz, Spain
[b] Université Catholique de Louvain, Louvain Drug Research Institute, Pharmaceutics and Drug Delivery, Brussels, Belgium

ARTICLE INFO

Article history:
Received 19 September 2012
Accepted 16 December 2012
Available online xxxx

Keywords:
Endocytosis
Transcytosis
Nanoparticle
P-gp substrate
Caco-2
M cell

ABSTRACT

The aims of this work were (i) to evaluate the potential of nanostructured lipid carriers (NLCs) as a tool to enhance the oral bioavailability of poorly soluble compounds using saquinavir (SQV), a BCS class IV drug and P-gp substrate as a model drug, and (ii) to study NLC transport mechanisms across the intestinal barrier. Three different NLC formulations were evaluated. SQV transport across Caco-2 monolayers was enhanced up to 3.5-fold by NLCs compared to SQV suspension. M cells did not enhance the transport of NLCs loaded with SQV. The size and amount of surfactant in the NLCs influenced SQV's permeability, the transcytosis pathway and the efflux of SQV by P-gp. An NLC of size 247 nm and 1.5% (w/v) surfactant content circumvented P-gp efflux and used both caveolae- and clathrin-mediated transcytosis, in contrast to the other NLC formulations, which used only caveolae-mediated transcytosis. By modifying critical physicochemical parameters of the NLC formulation, we were thus able to overcome the P-gp drug efflux and alter the transcytosis mechanism of the nanoparticles. These findings support the use of NLCs approaches for oral delivery of poorly water-soluble P-gp substrates.

1. Introduction

Most of newly discovered chemical entities are poorly soluble in water [1–4]. Enhancing the oral bioavailability of these poorly water-soluble compounds is of great interest to the scientific community and a key area of pharmaceutical research. One of the most widely studied strategies in this regard is nanotechnology [2,5–8], because of the ability of nanoparticles to pass multiple biological barriers and to release a therapeutic compound within the optimal dosage range. Polymeric nanoparticles [9], lipid nanocarriers [10–12], micelles [13,14], and nanosuspensions [5,15] appear to be promising tools for delivery of poorly soluble drugs, yet few have been commercialized.

Among the wide variety of current nanocarriers, solid lipid nanoparticles (SLNs) present certain advantages compared to other colloidal systems, including that they can be prepared without an organic solvent and using suitable large scale production method (e.g., high pressure homogenization) [16]. However, SLNs have a relatively low loading capacity for several drugs compared to other nanocarrier systems, and are associated with possible expulsion of the drug during storage, and have a high water content. Nanostructured lipid carriers (NLCs) are a second generation of SLNs, which have a solid matrix mixed with a liquid lipid (oil) to form an unstructured matrix that helps increase the drug loading capacity of nanoparticles and avoids or reduces drug expulsion from the matrix during storage [17,18].

Nanoparticle size and surface properties, among other physicochemical properties of nanoparticles, strongly influence the mechanisms involved in nanoparticle cell internalization [19–21]. The non-phagocytic pathways, involving clathrin-mediated endocytosis, caveolae-mediated endocytosis and macropinocytosis, are the most common mechanisms of nanoparticle absorption/transcytosis by the oral route [22]. Nevertheless, designing tunable nanocarriers in order to control the endocytic pathway remains a challenge. Increasing our understanding of the mechanisms and processes involved in nanoparticle transport across the intestinal barrier and the factors limiting their transport across this barrier could help improve the formulations to enhance drug absorption [23–26]. Improved knowledge of these processes can help them fulfill their potential as tools for delivery of poorly water-soluble drugs by the oral route and provide new insights in their potential application for the treatment of different pathologies using this route.

The aim of this work was, first, to evaluate NLCs as tools to enhance the oral bioavailability of poorly water-soluble compounds using saquinavir (SQV), a class IV drug in the Biopharmaceutical Classification System (BCS), and a P-glycoprotein (P-gp) substrate,

* Corresponding authors at: Université Catholique de Louvain, Louvain Drug Research Institute, Pharmaceutics and Drug Delivery Avenue Mounier 73 B1.73.12, 1200 Brussels, Belgium. Tel.: +32 2 7647320; fax: +32 2 7647398.
E-mail addresses: anne.desrieux@uclouvain.be (A. des Rieux), veronique.preat@uclouvain.be (V. Préat).

0168-3659/$ – see front matter © 2012 Published by Elsevier B.V.
http://dx.doi.org/10.1016/j.jconrel.2012.12.021

as a model drug and, second, to study NLC transport mechanisms across the intestinal barrier. We evaluated SQV transport and then conducted a mechanistic study of NLC transport across an in vitro Caco-2 model, simulating the enterocyte barrier, and a Caco-2/Raji cell M inverted coculture model simulating, the intestinal follicle-associated epithelium (FAE model) [27]. The influence of controversial parameters that could affect nanoparticle transport, such as the size and the surfactant content of the aforementioned nanoparticles, was investigated and their contribution to nanoparticle endocytosis and transcytosis was evaluated using endocytosis inhibitors. Finally, the ability of these nanocarriers to overcome P-gp efflux was also assessed.

2. Materials and methods

2.1. Materials

Saquinavir mesylate (SQV) was kindly provided by Roche (Mannheim, DE). Verapamil, chlorpromazine, nystatin, methyl-ß-cyclodextrin (MßCD), lovastatin, coumarin-6, Rose Bengal and propidium iodide (PI) were purchased from Sigma-Aldrich (St. Louis, MO). Precirol ATO®5 was kindly provided by Gattefossé (Madrid, SP). Tween 80 was purchased from Vencaser (Bilbao, SP). Poloxamer 188 was a gift from BASF (Madrid, Spain). Miglyol 812N/F was purchased from Sasol (Hamburg, DE). Potassium dihydrogen phosphate (KH_2PO_4) and disodium hydrogen phosphate (Na_2HPO_4) were obtained from Merck (Darmstadt, DE). Acetonitrile (gradient HPLC grade) was purchased from VRW (Leuven, BE).

2.2. Preparation of the formulations

2.2.1. NLC preparation

SQV-NLCs were prepared using the high pressure homogenization technique [28]. Briefly, Precirol ATO®5 (5 g), Miglyol 812 (0.5 mL) and SQV (50 mg) were blended and melted at 75 °C until a uniform and clear oil phase was obtained. The aqueous phase was prepared by dispersing Tween 80 (2%) (w/v) and poloxamer 188 (1%) (w/v) or Tween 80 (1%) (w/v) and poloxamer 188 (0.5%) (w/v) in water (50 mL) and heating to the same temperature as the lipid phase. The hot aqueous phase was then added to the oil phase and the mixture was sonicated for 15 s to form a hot pre-emulsion, which was subsequently homogenized at 80 °C and 500 bar using a Stansted nG12500 homogenizer (SFP, Essex, UK) for ten homogenization cycles. To obtain NLCs with an increased particle size, one of the batches was not homogenized and the pre-emulsion was used.

To track the entry of nanoparticles into the cells, SQV-NLCs were labeled with the fluorescent dye coumarin-6. Briefly, 5 mg of coumarin-6 was incorporated in the lipid phase of the formulation and the preparation continued as aforementioned.

2.2.2. SQV suspension

To evaluate free SQV transport compared to nanoparticle transport, an SQV suspension was prepared. SQV (50 mg) was dispersed in a transport buffer (Hank's Balance Solution Buffer, HBSS) (50 mL). The concentration of SQV was calculated by dissolving the SQV suspension in acetonitrile and analyzing the resultant solution by HPLC.

2.3. NLC characterization

2.3.1. Size and zeta potential measurements

The size of the NLCs was determined using photon correlation spectroscopy (PCS) and the zeta potential was measured using Laser Doppler Velocimetry (LDV) with a Malvern Zetasizer Nano ZS (Malvern Instruments Ltd., Worcestershire, U.K). Samples were diluted in MilliQ™ water before measurement.

2.3.2. Surface hydrophobicity of nanoparticles

The surface hydrophobicity of the NLCs was evaluated using the Rose Bengal method [29]. Briefly, increasing nanoparticle concentrations were diluted to a constant 20 μg/mL of Rose Bengal solution. The surface of the nanoparticles and the aqueous phase were considered as two phases. The absorption of the hydrophobic dye to the nanoparticle surface was measured by calculating the partitioning coefficient (PQ). The PQ values were plotted versus the increasing nanoparticle concentrations. The surface hydrophobicity of the nanoparticles was quantified by the slope of the line. The slope increases with increasing surface hydrophobicity.

2.3.3. Drug encapsulation efficiency

The encapsulation efficiency (EE) of SQV-NLCs was calculated by determining the amount of free drug using a filtration technique. The SQV-NLC suspension was placed in the upper chamber of Amicon® centrifugal filters (molecular weight cutoff, MWCO, 100,000 Da, Millipore, Spain) and centrifuged for 20 min at 1500 g. The unencapsulated SQV in the filtrate was determined using HPLC. The total drug content in the SQV-NLCs was determined by dissolving the SQV-NLCs in acetonitrile to release trapped SQV. The resulting solution was analyzed using HPLC. The drug loading content was the ratio of incorporated drug to lipid (w/w).

Encapsulation efficiency and drug loading, each determined in triplicate, were calculated as follows:

$$EE(\%) = \frac{Amount\ of\ SQV\ in\ NLCs}{Initial\ amount\ of\ SQV} x100$$

$$\text{Drug loading}(\%) = \frac{Amount\ of\ SQV\ in\ NLCs}{Amount\ of\ lipid\ in\ NLCs} x100.$$

Coumarin-6 encapsulation was assessed by ultracentrifuging coumarin-6-SQV-loaded NLC suspension (1500 g, 20 min) using Millipore (Madrid, Spain) Amicon® ultra centrifugal filters (molecular weight cutoff, MWCO, 100,000 Da). Free coumarin-6 present in the filtrate was then measured using fluorimetry (SFM 25 fluorometer, Konton Instruments).

2.3.4. Determination of saquinavir by HPLC

HPLC for SQV was performed with a Waters 1525 HPLC Binary Pump (Waters Corp., Milford, USA). The detector was a Waters 2487. The system was controlled by Breeze software (Waters, UK). A Nucleodur 100-5 C18 5 μm (4 mm × 125 mm) was used at room temperature. The mobile phase contained 46% acetonitrile and 54% (v/v) of 70 mM KH_2PO_4 was adjusted to pH 5 with 80 mM Na_2HPO_4, as previously reported by Albert et al. [30]. The flow rate was set at 1 mL/min in isocratic elution and the injected sample volume was 50 μL, except for the analysis of SQV under certain inhibitors for which a sample volume of 100 μL was necessary to reach the limit of quantification. The assay was linear over the SQV concentration range of 0.025–15 μg/mL. The intra- and inter-day coefficients of variation were both within ±5%. The limits of detection (LOD) and of quantification (LOQ) of SQV were 0.0125 μg/mL and 0.025 μg/mL, respectively. No interfering peaks were detected within the assay.

2.4. In vitro dissolution assay

The in vitro dissolution assay was performed in HBSS (transport buffer during the in vitro assays) using Quix-Sep® cells (Membrane Filtration Products. Inc., TX, USA) at 37 °C under magnetic stirring. A dialysis regenerated cellulose membrane with an MWCO between 6000 and 8000 Da was used. The membrane was first soaked in medium for 24 h before placing it in a Quix-Sep® cell. Five hundred microliters of the SQV-NLC suspension was placed in the cell and introduced into a 200 mL of HBSS. After 2 h, samples were

Please cite this article as: A. Beloqui, et al., Mechanism of transport of saquinavir-loaded nanostructured lipid carriers across the intestinal barrier, J. Control. Release (2012), http://dx.doi.org/10.1016/j.jconrel.2012.12.021

withdrawn from the medium and analyzed by HPLC using the above mentioned method. The dissolution test was carried out in triplicate for each formulation under sink conditions.

In addition, in order to assess the stability of the nanoparticles in the gastrointestinal tract, the in vitro dissolution assay was performed in simulated gastric fluid (SGF) and in simulated intestinal fluid (SIF) as described in the European Pharmacopeia (European Pharmacopeia, 2010) and performed as abovementioned. Samples were withdrawn after 2 h and 8 h in SGF and SIF, respectively.

2.5. In vitro culture studies

2.5.1. Cell cultures: Caco-2 and FAE monolayers

All cell culture media and reagents were purchased from Invitrogen (Merelbeke, BE). Caco-2 cells (clone 1) were kindly provided by Dr Maria Rescigno, University of Milano-Bicocca (Milano, Italy) [31] and used from passage $x+12$ to $x+30$. Human Burkitt's lymphoma Raji B cell line was purchased from American Type Culture Collection (Manassas, VA, USA) and used between passages 102–110. Caco-2 cells were grown in DMEM supplemented with 10% (v/v) inactivated fetal bovine serum, 1% (v/v) non-essential amino-acids, and 1% (v/v) L-glutamine, at 37 °C under a 10% CO_2/90% air atmosphere. Caco-2 cells were grown on inserts in the same medium, but further supplemented with 1% (v/v) of penicillin–streptomycin (PEST). Raji cells were grown in a suspension culture, cultivated in RPMI medium supplemented with 10% (v/v) inactivated fetal bovine serum, 1% (v/v) non-essential amino-acids, 1% (v/v) L-glutamine, and 1% (v/v) PEST, at 37 °C in a 5% CO_2/95% air atmosphere.

Caco-2 cells were seeded at a density of 5×10^5 cells/well on Transwell® polycarbonate inserts (12 mm insert diameter, 3 μm pore size) (Corning Costar, Cambridge, U.K.) and cultivated over 21 days. The medium was replaced every second day. The inverted FAE model was obtained by co-culturing Raji and Caco-2 as previously reported by des Rieux et al. [27,32]. Briefly, after 3 to 5 days of Caco-2 seeding, inserts were inverted, a piece of silicone tube was placed into the inserts and maintained until day 21 in large Petri dishes. The medium was replaced every other day, until day 9–11 when Raji cells were then added to the basolateral compartment for the conversion of Caco-2 cells into M cells at a density of 2.5×10^5 cells/well.

2.5.2. Cytotoxicity studies

Cell viability was assessed after the co-incubation of 20,000 Caco-2 cells/well on a 96-well tissue culture plate (Costar® Corning® CellBIND Surface) with the aforementioned formulations in dispersion in culture medium. After 2 h of incubation, the supernatants of each well were removed and preserved at 4 °C for the LDH assay and the cells were incubated again for 3 h with 100 μL 0.5 mg/mL 3-(4,5-dimethylthiazol-2-yl)-(2,5-diphenyltetrazolium bromide) (Sigma-Aldrich, BE) (MTT assay). The measurement of lactate dehydrogenase (LDH) activity released from the cytosol of damaged cells (LDH assay) (Roche Diagnostics Belgium, Vilvoorde, BE) was performed following manufacturer's instructions [33].

The IC_{50}s for the different formulations were calculated using the GraphPad Prism 5 program (CA, USA). All MTT assays were repeated in triplicate.

The LDH release induced by the different nanoparticles did not exceed 25%, even for the highest concentration.

The integrity of the monolayer was also corroborated by measuring the trans-epithelial electrical resistance (TEER) before and after the transport studies on day 21. The measurements were carried out at 37 °C using an epithelial voltohm meter (EVOM, World Precision Instruments, Berlin, DE). Monolayers with TEER values over 200 $\Omega\,cm^2$ for Caco-2 monolayers and over 100 $\Omega\,cm^2$ for the FAE model were used. TEER values after transport studies were not significantly different to initial values unless otherwise stated.

2.5.3. Evaluation of SQV permeability across intestinal in vitro models

The permeability of SQV across gastrointestinal in vitro models was evaluated by comparing free SQV with SQV-NLC formulations, in Caco-2 cells and in the FAE monolayers.

The experiments were conducted at 37 °C or 4 °C by adding a volume of 400 μL at 44 μg/mL SQV concentration in HBSS on the apical side and 1 mL of HBSS on the basolateral side. After 2 h of incubation, samples were collected from the basolateral side and SQV concentration was measured by HPLC: The apparent permeability coefficient (P_{app}, cm s^{-1}) was calculated according to the following equation [23,24]:

$$P_{app} = dQ/dt \times 1/AC_0$$

where dQ/dt is the transport rate (μg/s), C_0 is the initial drug concentration on the apical side (μg/mL), and A is the surface area of the membrane filter (cm^2).

After transport experiments, cell monolayers were washed twice in cold HBSS and fixed in paraformaldehyde (PFA) 4% for subsequent staining.

For the assessment of FAE model functionality in each experiment transport studies was conducted under the aforementioned conditions with commercial fluorescent carboxylated nanoparticles (0.2 μm) (Gentaur, BE) [26,34]. A nanoparticle suspension (400 μL) with final concentration of 4.5×10^9 nanoparticles/mL was added on the apical side and inserts were incubated at 37 °C for 2 h. After this incubation time, basolateral solutions were then sampled and the number of transported nanoparticles was measured using a flow cytometer (BD FACSCalibur). Nanoparticle transport was expressed as mean ± SD.

2.5.4. Mechanisms of transport of SQV-NLCs across Caco-2 cells

In order to evaluate the endocytosis mechanisms involved in SQV-NLC transport across Caco-2 cells, the monolayers were pre-incubated for 1 h at 37 °C with 400 μL of a solution consisting of different concentrations of endocytosis inhibitors in transport buffer. After 1 h, SQV-NLC was added into the inhibitor solution on the apical side and co-incubated for 2 h. Chlorpromazine of 10 μg/mL was used as an inhibitor of receptor-mediated and clathrin-mediated endocytosis [23,24]. The endocytic pathway of caveolae/lipid raft mediated endocytosis was inhibited with nystatin of 50 μg/mL [35,36]. MßCD 10 mM (13.2 mg/mL) in the presence of lovastatin 1 μg/mL, an inhibitor of de novo synthesis of cholesterol [37], was used for the inhibition of caveolae and clathrin-mediated pathways by cholesterol depletion [37].

As mentioned previously, SQV is a well-known P-gp substrate [38,39]. To evaluate the role of SQV-NLCs in the inhibition of P-gp, cells were pretreated with a solution of 100 μM verapamil, a well-known P-gp inhibitor [39,40], for 1 h and nanoparticles were subsequently added on the apical side and incubated for 2 h in the presence of verapamil. The evaluation of SQV suspension P_{app} was also carried out under P-gp inhibition to confirm that SQV was a P-gp substrate in our Caco-2 cell model.

In all the assays carried out in the presence of inhibitors, several inserts were kept as controls and the transport studies were carried out in transport buffer instead of in inhibitor solutions.

2.5.5. Intracellular uptake of nanoparticles by Caco-2 cells

Entry of nanoparticles into Caco-2 cells was studied quantitatively by flow cytometry and qualitatively by confocal laser scanning microscopy (CLSM), for which coumarin-6 ($\lambda_{em}=505$ nm) loaded nanoparticles were employed.

For the flow cytometry study, Caco-2 cells were seeded in 24-well cell culture plates at a density of 5×10^5 cells per well and allowed to adhere for 48 h until confluency. As for the transport studies, cells were co-incubated with 400 μL of a coumarin-6 loaded nanoparticles suspension in transport buffer (17.5 μL per 100 μL of buffer). After 2 h of incubation with fluorescent nanoparticles, cells were washed three

times with PBS and detached from the plates by trypsinization. Cells were then centrifuged at 1500×g, the supernatant was discarded, the cells were resuspended in PBS and fluorescence was measured using a BD FACSCalibur flow cytometer and BD CellQuest software (Becton Dickinson Biosciences, San Jose, CA, US). Cell fluorescence was quantified by measuring the fluorescence of coumarin-6 at 525 nm (FL1). To avoid fluorescence overestimation inside the cells from free dye entry, coumarin-6 was added as a solution (100 μg/mL) and prepared as described by Rivolta et al. [41]. For cell viability measurements, the propidium iodide reagent was employed. The reagent was added to each sample at a final concentration of 10 μg/mL, and, after 10 min of incubation, the fluorescence corresponding to dead cells was measured at 620 nm (FL2). For each sample, 10,000 events were collected. The data were subsequently analyzed using the FlowJo data analysis software package (TreeStar, USA). In the case of inhibition studies, cells were pre-treated 1 h with the inhibitors used for the transport mechanisms studies (Section 2.5.4).

For the CLSM study, the Transwell® inserts fixed in PFA 4% were gently washed in HBSS. Actin was stained with 200 μL of rhodamine–phalloidine (1:50) in buffered HBSS + 0.2% (v/v) Triton X-100 for 10 min in the dark to reveal cell borders, as described by des Rieux et al. [26]. Cell nuclei were stained with DAPI (1:20). Subsequently, inserts were washed in HBSS, cut and mounted on glass slides. Images were captured using a Zeiss™ confocal microscope (LSM 150). Data were analyzed by the Axio Vision software (versus 4.8) to obtain *y–z*, *x–z* and *x–y* views of the cell monolayers.

2.6. Statistical analysis

Statistical analysis was performed using the GraphPad Prism 5 program (CA, USA). Normal distribution was assessed with the Shapiro–Wilk normality test. One-way ANOVA in multiple comparisons followed by Tukey's post-hoc test was applied according to the result of the Bartlett's test of homogeneity of variances for the 37 °C and 4 °C transport comparisons. All other analyses were performed using a Student's *t*-test. Differences were considered statistically significant at $^{*}p<0.05$. Results are expressed as mean ± SD.

3. Results and discussion

3.1. NLC characterization

Three lipid formulations differing in particle size and surfactant content were obtained, all negatively charged. Particle characterization and compositions of the different formulations are summarized in Table 1. The composition of these nanoparticles was based on results from previous studies on lipid nanoparticles carried out in our laboratory [42].

All the formulations had an EE of ~100% and drug loading of ~0.90%. Reduction in the amount of surfactant present in the formulation leads to an increased particle size (165 ± 6 nm versus 247 ± 4 nm for formulations A and B, respectively). Moreover, when formulation B was prepared without further homogenization (formulation C), the particle size varied from the nanometer to the micrometer range (247 ± 4 nm versus 1090 ± 6 nm for formulations B and C, respectively), highlighting the importance of the preparation method in obtaining different nanoparticle sizes. Although SQV is considered a model drug, the low drug loading of SQV (~0.90%; therapeutic dose 1 g twice a day) compromises the foreseen application of these nanocarriers to reach an efficient therapeutic effect of the drug and it would be desirable to encapsulate more potent drugs with a lower therapeutic dose (e.g. budesonide, 9 mg once a day in Crohn's disease).

There were no differences in nanoparticle parameters and EE of SQV when incorporating coumarin-6 (5 mg) into the formulations (data not shown). There was a difference in nanoparticle surface hydrophobicity between the three formulations: formulation A had a higher slope and, thus, higher hydrophobicity compared to formulations B and C. Formulations B and C had the same amount of surfactant but formulation B had higher hydrophobicity than formulation C, which can be explained by the different surface areas of the two formulations [29].

Table 1
Summary of formulation composition and particle size, zeta potential and polydispersity index (P. I.) per formulation (n = 3; data are expressed as mean ± SD).

		NLC formulations		
		A	B	C
Composition	Tween 80 (g)	1	0.5	0.5
	Poloxamer 188 (g)	0.5	0.25	0.25
	Precirol ATO® 5 (g)	5	5	5
	Mygliol 812N/F (mL)	0.5	0.5	0.5
	SQV (mg)	50	50	50
	H_2O (mL)	50	50	50
	Homogenization	Yes	Yes	No
Characterization	Size (nm)	165 ± 6	247 ± 4	1090 ± 6
	Zeta (mV)	−21 ± 8	−33 ± 7	−31 ± 5
	P. I.	0.16	0.35	0.6
	Surface hydrophobicity (slope)	0.054	0.040	0.008
	EE (%)	99 ± 0.2	99 ± 0.02	99 ± 0.14
	Drug loading (%)	0.90 ± 0.00	0.90.00	0.90.00

3.2. In vitro dissolution assays

An in vitro dissolution study was performed to ensure that SQV was not released from the NLC formulations during the in vitro transport studies. The amount of drug released from the NLCs into the transport buffer medium (HBSS) during 2 h of incubation at 37 °C was analyzed by HPLC (n = 3). For the three formulations, SQV release was less than 0.4% indicating that the differences in the subsequent data were not the result of greater dissolution (maximum solubility of SQV mesylate in HBSS ~50 μg/mL [43]).

Moreover, for the three formulations, the drug released from NLCs in SGF media after 2 h of incubation at 37 °C was below the LOD (LOD<0.0125 μg/mL) (n = 3). SQV release was below the LOD after 2 h and less than 5% in SIF media after 8 h of incubation at 37 °C (n = 3).

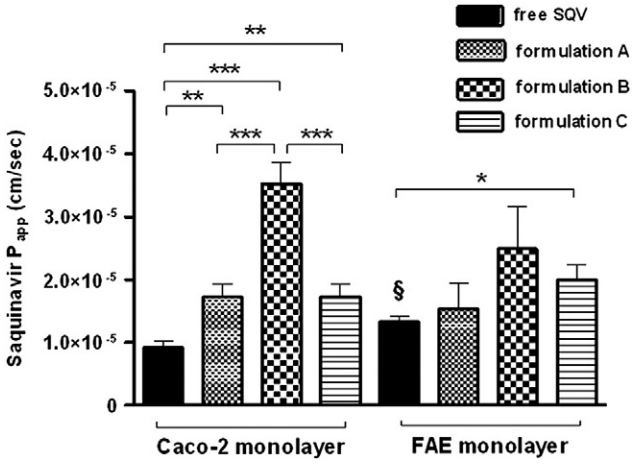

Fig. 1. Saquinavir (SQV) P_{app} values obtained after 2 h of incubation of the three NLC formulations (A, B and C) and a SQV suspension in the Caco-2 monolayers and the FAE monolayers. (n = 9, mean ± SD, $^{*}p<0.05$, $^{**}p<0.01$, $^{***}p<0.001$). $^{§}p<0.05$ versus Caco-2 monolayers.

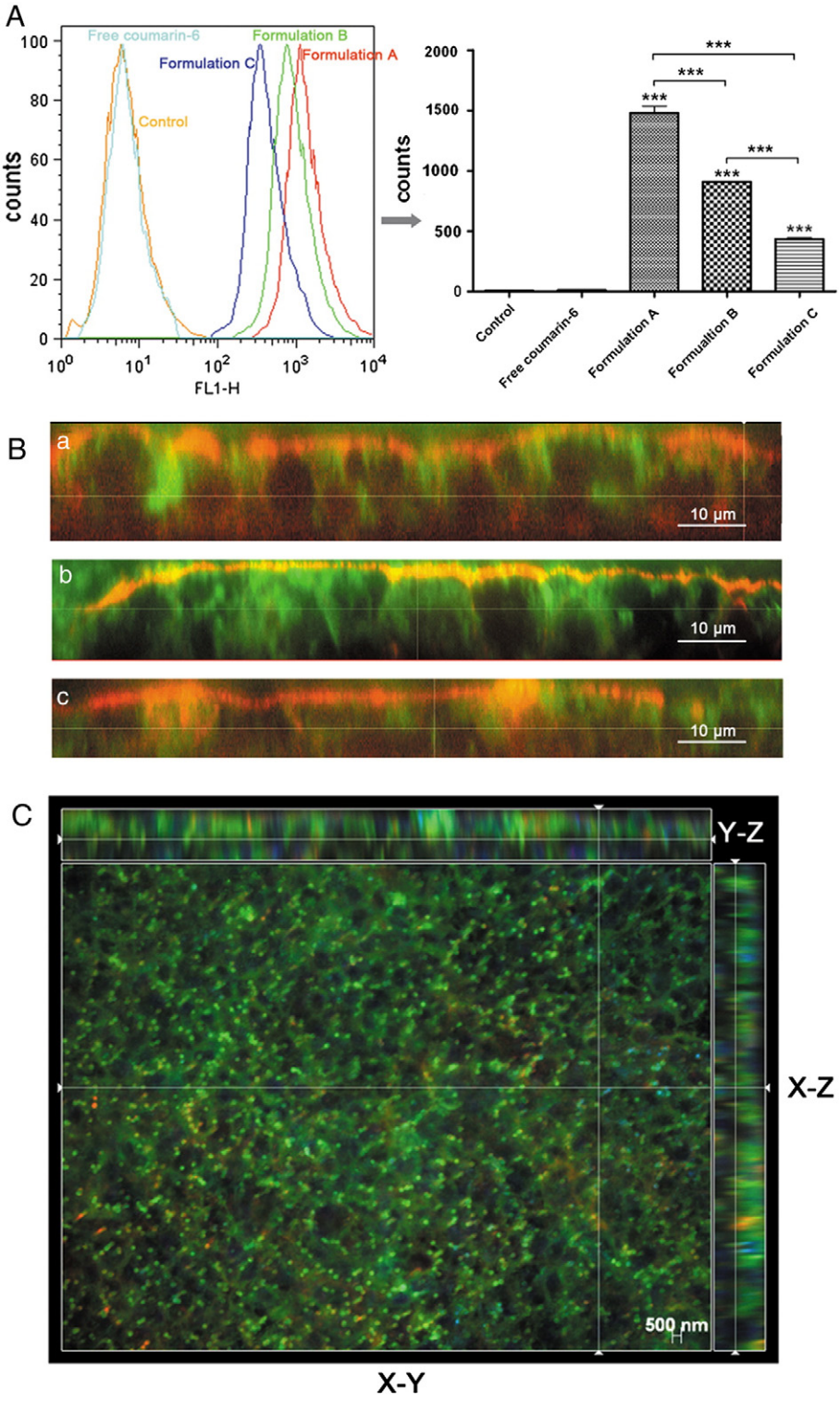

Q2 **Fig. 2.** Cellular uptake of coumarin-6 NLCs (green) in Caco-2 cells, measured by flow cytometry, (A) and CLSM images (B and C) of the inserts after 2 h of incubation with the nanoparticles. A) Nanoparticles and free coumarin-6 entrance into the cell measured by flow cytometry. Untreated cells are shown as control ($n = 3$; ***$p < 0.001$). B) a, b and c correspond to *y–z* sections of CLSM images of the inserts for formulations A, B and C, respectively. Cell membranes are stained in red with rhodamine–phalloidine and cell nuclei in blue with DAPI. C) *y–z*, *x–y* and *x–z* sections of formulation A CLSM images with which the higher uptake rate was recorded. (For interpretation of the references to color in this figure legend, the reader is referred to the web version of this article.)

3.3. In vitro evaluation of SQV transport across the intestinal barrier

3.3.1. SQV permeability evaluation across Caco-2 monolayers and FAE monolayers

The main aim of the present study was to evaluate the potential of NLCs as suitable carriers for poorly water-soluble drugs using SQV as a BCS class IV model drug. For this purpose, the permeability of SQV across the enterocyte-like model (Caco-2 monolayers) and the FAE monolayers (Caco-2/Raji cell coculture) was evaluated. The conversion of Caco-2 cells into M-cells in the FAE model was confirmed by measuring the number of commercial carboxylated particles transported using a flow cytometer. After 2 h of incubation, the number of transported

nanoparticles was significantly higher in the FAE model than in the Caco-2 model (82,633 ± 6443 nanoparticles, versus 108 ± 91, respectively; n = 4, $p<0.05$).

The permeability values obtained for each nanoparticle formulation were compared with the permeability values of free SQV as a suspension. Fig. 1 represents the P_{app} of SQV data obtained for the assayed formulations after 2 h of incubation in Caco-2 monolayers and in FAE monolayers.

In the Caco-2 model, the increase in SQV P_{app} values for the nanoparticle formulations compared to free SQV, is highlighted. It is remarkable to note the 3.5-fold increase in the SQV P_{app} with formulation B compared to free SQV ($p<0.001$), and the 2-fold increase compared with the two other NLC formulations (A and C) ($p<0.01$). These SQV P_{app} values are greater than previously reported values obtained across Caco-2 monolayers and ex vivo transport studies using different strategies for enhancing SQV permeability [44,45]. These data confirm that NLCs are suitable carriers for enhancing the permeability of poorly water-soluble drugs. There was a significant difference between the P_{app} values of formulations B (247 ± 4 nm) and C (1090 ± 6 nm) ($3.52\times10^{-5}\pm3.34\times10^{-6}$ cm/s versus $1.73\times10^{-5}\pm2.09\times10^{-6}$ cm/s, respectively; n = 9, ***$p<0.001$).

In the M cell model, there was a significant increase in the P_{app} of formulation C compared to free SQV in suspension ($p<0.05$), which was not observed for formulations A or B ($p>0.05$). Enhanced microparticle uptake by M cells has been previously reported [46,47]. In contrast to polymeric nanoparticles [32], the permeability of the drug from the submicron NLCs was not increased in M cells. Hence, the subsequent evaluation of the transport mechanisms and the intracellular uptake was evaluated only in the Caco-2 cell model.

The diffusion of the particles through the mucus could also affect their transport [48]. Peyer's patches, in particular M cells, are less protected by the mucus barrier but account for only 1% of total surface area. The mucus penetrating properties of lipid-based nanoparticles, including NLCs, have not been extensively studied. NLCs are small enough (formulations A and B) to avoid being blocked sterically in the mucin mesh. However, as the mucus is rich in lipids, mucoadhesion of the NLCs could be promoted by their hydrophobic surface even if the surfactant coating could make their surface partly hydrophilic and more mucus penetrating. Mucus interaction with NLCs should be investigated.

3.3.2. Intracellular uptake in Caco-2 cells

Fig. 2 shows the flow cytometry results (Fig. 2A) and the CLSM images (Fig. 2B and C) corresponding to the cellular uptake of the nanoparticle formulations and free coumarin-6. Cell viability was assessed by staining dead cells with PI and was greater than 90% in all cases unless otherwise stated. Untreated cells were used as controls.

The cellular uptake of NLCs was size-dependent (formulation A > B > C; n = 3, ***$p<0.001$; Fig. 2A). This finding is consistent with Rejman et al. [19] who also reported a tendency to decreased internalization with increased particle size. These authors studied the pathway of entry and subsequent fate of commercial latex nanoparticles inside the cell and concluded that particles with a diameter of <200 nm enter the cell via clathrin-mediated endocytosis whereas larger particles (200 nm–1 μm) enter preferentially via caveolae-mediated endocytosis. Moreover, the surface hydrophobicity of the nanoparticles may also determine nanoparticle entrance into Caco-2 cell because the larger uptake into the cells is correlated with the higher nanoparticle surface hydrophobicity (formulation A > B > C) [27]. Gaumet et al. [21] found that the surface hydrophilicity of polymeric nanoparticles was a critical factor for nanoparticle uptake and Liang et al. [49] reported that gold nanoparticles were more efficiently taken up with increasing hydrophobic interactions with the membrane of Caco-2 cells. In our study, nanoparticle size and surface hydrophobicity were major factors influencing NLC entrance into the cell.

The P_{app} values for SQV formulated in NLCs did not correlate with their intracellular uptake. Formulation B exhibited higher SQV P_{app} values than did formulations A and C but did not have a higher intracellular uptake. Fig. 2B shows that NLCs penetrated inside the Caco-2 cells whatever is the formulation.

3.3.3. Mechanistic study of SQV-NLC transport across Caco-2 cells

3.3.3.1. Influence of the temperature on NLC transport. The second objective of the present study was to evaluate the mechanisms of transport used by the different NLC formulations to estimate whether the differences on permeability were due to different entry pathways. For this purpose, we first focused on the type of transport: passive or active. Although lipid nanoparticles are known to enter into cells in an active endocytic manner [24], we assessed this phenomenon in Caco-2 cells and the FAE model. It is well-established that at 4 °C pinocytic/endocytic uptake is inactivated [50]. Fig. 3 illustrates the influence of temperature on the transport of SQV-loaded nanoparticles and SQV suspension across Caco-2 and FAE monolayers. In most cases, SQV was not detected in the basolateral side after nanoparticle incubation at 4 °C (LOD < 0.0125 μg/mL). These data suggest that SQV loaded in NLCs might mainly permeate Caco-2 cells and FAE monolayers in an active manner.

3.3.3.2. Characterization of NLC endocytosis mechanisms. Taking the aforementioned results together, we can conclude that NLCs predominantly enter cells by endocytosis. Different mechanisms of nanocarrier internalization in cells have been described: macropinocytosis, clathrin-mediated endocytosis, caveolae-mediated endocytosis and clathrin- and caveolae-independent endocytoses [22]. To evaluate the endocytic mechanism used by NLCs, transport studies were undertaken in the presence of different inhibitors. We quantified the intracellular uptake, measured by flow cytometry, and the permeability of SQV across Caco-2 cells by HPLC after the transport study.

Fig. 4 represents the intracellular uptake of coumarin-6-SQV-loaded NLCs in Caco-2 cells after 2 h of incubation along with chlorpromazine, an inhibitor of clathrin-mediated endocytosis [23,24], nystatin, an inhibitor of caveolae/lipid raft-mediated endocytosis [35,36] and MßCD + lovastatin, an inhibitor of both clathrin- and caveolae-mediated endocytoses [37].

There was no significant difference in the presence of clathrin- or caveolae-mediated endocytosis inhibitors (chlorpromazine and nystatin, respectively) regardless of the nanoparticle formulation. In contrast, there was a significant difference when the cells were incubated in the presence of MßCD and lovastatin. It has to be remembered that, by sequestering cholesterol, is not only caveolae integrity disrupted but also other endocytic mechanisms involving cholesterol [51,52], so that clathrin- and caveolae-independent cholesterol-dependent

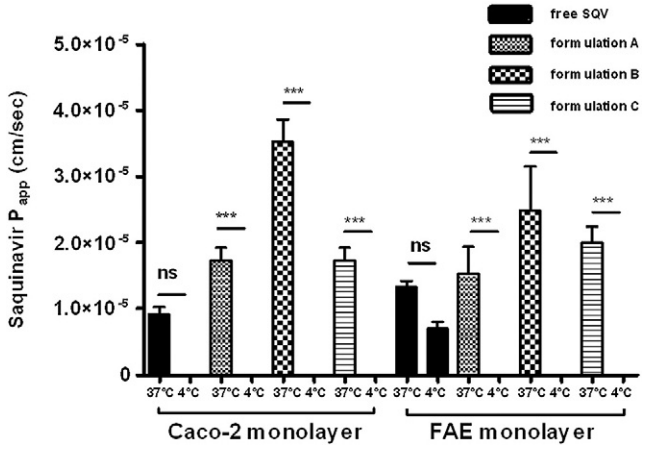

Fig. 3. Influence of temperature on nanoparticle and free SQV transport in Caco-2 and FAE monolayers after 2 h of incubation at 37 °C and 4 °C. (n = 9; ***$p<0.001$) (ns: no significant difference).

Please cite this article as: A. Beloqui, et al., Mechanism of transport of saquinavir-loaded nanostructured lipid carriers across the intestinal barrier, J. Control. Release (2012), http://dx.doi.org/10.1016/j.jconrel.2012.12.021

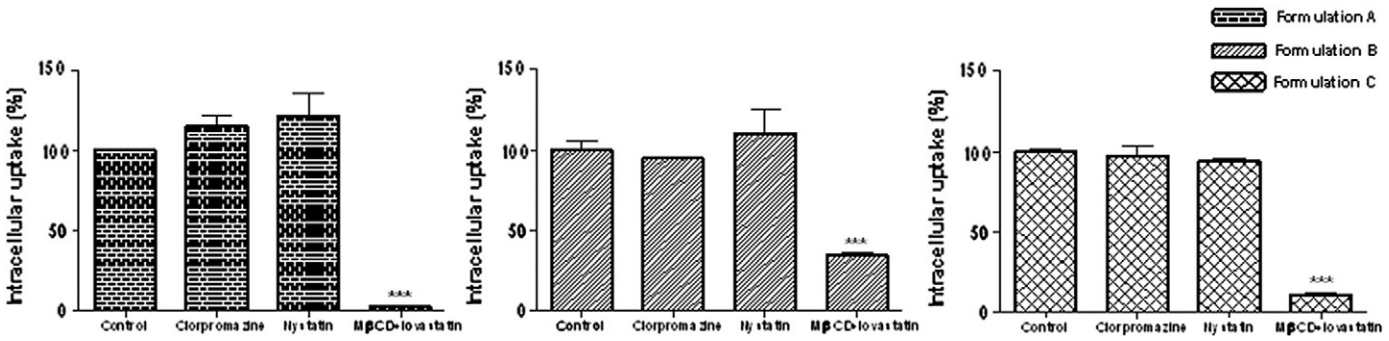

Q6 **Fig. 4.** Intracellular uptake, measured by FACS, of coumarin-6-SQV-loaded NLCs in Caco-2 cells after 2 h of incubation with inhibitors. Formulations under no inhibition were considered as controls and represent P_{app} values of 100%. (n = 3, ***p < 0.001).

mechanisms may be involved in NLC endocytosis [53]. Furthermore, clathrin-independent endocytosis has been related to so called *lipid rafts*, lipid-based cholesterol-enriched microdomains present on certain cell surfaces. Whether caveolae and rafts share a common pathway remains controversial [54–56], but both are undoubtedly sensitive to cholesterol depletion and share common machinery. Paillard et al. [57] also reported a significant decreased in internalization of lipid nanocapsules under MßCD and lovastation inhibition regardless of nanoparticle size, suggesting that endogenous cholesterol was involved in lipid nanoparticle internalization. Although no significant differences were found regarding nystatin inhibition or chlorpromazine, during the intracellular uptake study, one should take into account the fact that the internalization process occurs under distinct mechanisms acting in parallel and, thus, the different endocytic pathways might tend to compensate each other [58]. This factor could explain, in part, why there were no significant differences in the endocytosis when incubating the nanocarriers with one of these specific inhibitors, but their involvement in nanoparticle internalization should not be totally discarded.

Cell viability was greater than 99% when compared to untreated cells in all cases except for formulation A co-incubated with MßCD + lovastatin for which viability was 65% (data not shown).

3.3.3.3. Transcytosis. It is important to distinguish between the mechanisms of endocytosis and transcytosis. Endocytosis involves the uptake or internalization of the nanoparticles inside the cells, whereas transcytosis is the transport across the cell from one membrane to the opposite. To evaluate the transcytosis of NLC formulations in the Caco-2 cell model, the nanocarriers were incubated in the Caco-2 cells monolayers along with the clathrin- and caveolae-mediated inhibitors, chlorpromazine and nystatin, respectively. After 2 h of incubation, SQV P_{app} was estimated and results were expressed as percentage of control values. The P_{app} value of SQV-loaded NLCs under no inhibition was considered as 100% (control). Fig. 5 features a diagram of SQV P_{app} after 2 h of incubation of SQV-loaded nanoparticles with chlorpromazine (Fig. 5A) or nystatin (Fig. 5B). SQV P_{app} was also evaluated under MßCD and lovastatin inhibition. The presence of these inhibitors induced TEER values of the monolayers less than 200 $\Omega\,cm^2$ after the transport study. Therefore, because we could not guarantee the integrity of the monolayer, these results were excluded and transcytosis was characterized exclusively under nystatin and chlorpromazine inhibitions. Permeability decreased significantly with caveolae/lipid rafts depletion in the presence of nystatin regardless of the formulation (Fig. 5B). Simionescu et al. [59] suggest that endocytosis and transcytosis share the same mechanisms (receptor-independent and receptor-mediated) and caveolae. Hence, regarding the results obtained under caveolae/lipid raft inhibiton and the existence of a caveolae transcytotic pool, caveolae vesicle-mediated transcytosis appears to be involved in SQV transcytosis across Caco-2 cells regardless of the nanocarrier. The same decreased permeability was observed under clathrin depletion exclusively in the case of formulation B (Fig. 5A), which means that clathrin is also involved in SQV transcytosis with this formulation. Roger et al. [24] also reported a clathrin- and caveolae-mediated internalization of paclitaxel-loaded lipid nanocapsules involved in the transcellular transport of the drug across Caco-2 cells, but in our study, in the case of NLCs, this was not a steady phenomenon and depended on nanoparticle size and the amount of surfactant employed in the formulation.

We relate the entry pathway of the nanocarriers with the transcytosis of the drugs itself, but we do not provide information about the fate of the nanoparticle inside of the cell as we did not assess the presence of the nanoparticles in the receiver compartment.

3.3.3.4. Evaluation of the contribution of P-gp inhibition to enhancement of SQV permeability. SQV is known to be a P-gp substrate [38]. To evaluate whether the NLCs inhibited the P-gp drug efflux, we conducted

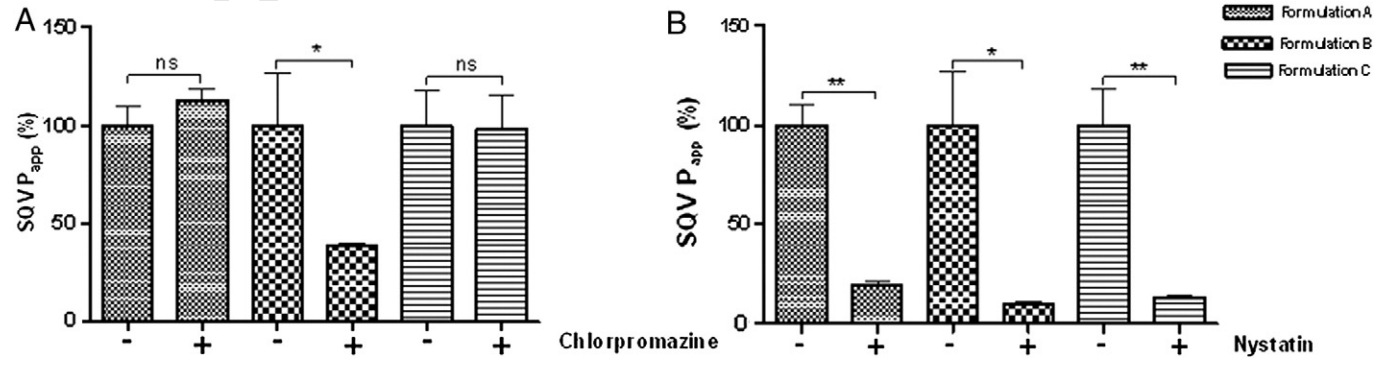

Fig. 5. Comparison of SQV P_{app} values under clathrin (A) and caveolae (B) inhibitions (chlorpromazine 10 μg/mL and nystatin 50 μg/mL, respectively) with untreated cell values (n = 3–5; *p < 0.05, **p < 0.01, ns: no significant difference). "−" absence of an inhibitor,"+" under inhibition.

Please cite this article as: A. Beloqui, et al., Mechanism of transport of saquinavir-loaded nanostructured lipid carriers across the intestinal barrier, J. Control. Release (2012), http://dx.doi.org/10.1016/j.jconrel.2012.12.021

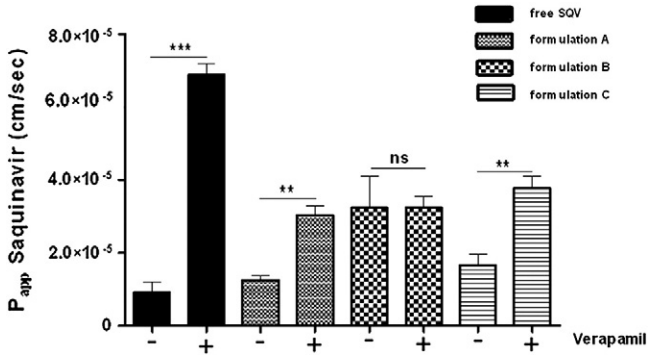

Fig. 6. SQV P_{app} values for free SQV and the nanoparticles after 2 h of incubation with 100 μM verapamil, a P-gp inhibitor (n = 9; ns: no significance; **p<0.01, ***p<0.001). Formulations with no inhibition were considered as controls (n = 3). "−" absence of verapamil, "+" under verapamil inhibition.

SQV permeability studies in Caco-2 cells under verapamil inhibition, a well-known P-gp inhibitor [40].

Fig. 6 shows SQV P_{app} values after 2 h of incubation in the presence of 100 μM verapamil, inhibiting P-gp, or in a transport buffer, without P-gp inhibition.

Our results confirm that SQV is a P-gp substrate. Indeed, incubating a SQV suspension with verapamil for 2 h significantly increased permeability (***p<0.001). Formulations A and C also exhibited greater permeability when the P-gp efflux was inhibited. In contrast, there was no difference in the permeability rates with formulation B regardless of the presence or absence of verapamil, suggesting that this formulation circumvented the P-gp efflux and, thus, enhanced SQV permeability. A shift in the internalization mechanism could explain how formulation B overcomes the P-gp efflux. In this study, it was already reported that a clathrin-mediated transcytosis in addition to a caveolae-mediated transcytosis for formulation B, were not present with formulations A and C. This finding could explain the ability of formulation B to circumvent the P-gp drug efflux. P-gp is localized in caveolae [60], where it is co-localized with Cav-1 [61], the principal component of caveolae. Several immunoprecipitation studies have suggested an interaction between P-gp and Cav-1 which could modulate P-gp transport activity. Barakat et al. [62] reported that decreased P-gp/Cav-1 interactions led to increased P-gp transport activity. Thus, one might hypothesize that, as clathrin-mediated endocytosis could contribute to the entrance of formulation B into the cell, there may be decreased competition for the caveolae pathway and, hence, increased P-gp/Cav-1 interaction and decreased P-gp activity. This ability of formulation B to overcome P-gp efflux could explain the 2-fold permeability increase found with formulation B in comparison to formulations A and C. Interestingly, the same formulation prepared by a different method and with a different size (247 ± 4 nm versus 1090 ± 6 nm; formulations B and C respectively) did not have the same ability to overcome the P-gp, highlighting the importance not only of the composition but also of the method employed for the preparation as it provided a different particle size.

Fig. 7 features a schematic representation of the NLCs A, B and C transports across Caco-2 cells.

Previous studies reported competition between lipid nanocapsules and P-gp for paclitaxel transport across Caco-2 cells describing P-gp inhibition by the nanoparticles themselves and suggesting that P-gp may not only be involved in drug efflux but also in the regulation of endocytosis [40]. However, the mechanisms used by these nanoparticles to inhibit the P-gp remained unclear. The mechanistic study allowed us to demonstrate the contribution of clathrin-mediated transcytosis of NLCs to circumvent P-gp, which resulted in a 2-fold increase in permeability of SQV, and highlights the importance of lipid nanoparticle size and composition on their ability to overcome the P-gp efflux.

These findings add to the large number of approaches for delivery of P-gp substrates using nanotechnology [63].

4. Conclusion

In this study, we evaluated three different NLC formulations and assessed their potential to increase drug permeability using SQV (a BCS class IV drug and P-gp substrate) as a model drug. NLCs enhanced SQV permeability up to 3.5-fold. SQV transport across the intestinal barrier was influenced by the size of the NLCs and the amount of surfactant used for their formulation. Transport of NLCs was not increased by M cells, in contrast to drug suspension. Formulation B (247 nm and 1.5% (w/v) of surfactant content) circumvented the P-gp efflux and used both a caveolae- and clathrin-mediated transcytosis, in contrast to formulations A and C, which followed caveolae-mediated transcytosis. By modifying critical physicochemical parameters of the formulation we were able to overcome the P-gp drug efflux and alter the transcytosis mechanism of the nanoparticles. To our knowledge, this is the first time that a mechanistic study of NLC transport across intestinal in vitro models has been described. Our findings are encouraging for the delivery of class IV drugs and P-gp substrates by the oral route and support further nanotechnology approaches on this regard.

Acknowledgments

A. Beloqui wishes to thank the University of the Basque Country UPV/EHU for the fellowship grants (Personal Investigador en Formación 2008 and Ayudas para la movilidad y divulgación de resultados de investigación en la Universidad del País Vasco, movilidad de investigadores en estancias 2011). This work was partially supported by the Basque Government's Department of Education, Universities and Investigation (IT-341-10) and *Fonds de la Recherche Scientifique Medical* (FRSM, Belgium).

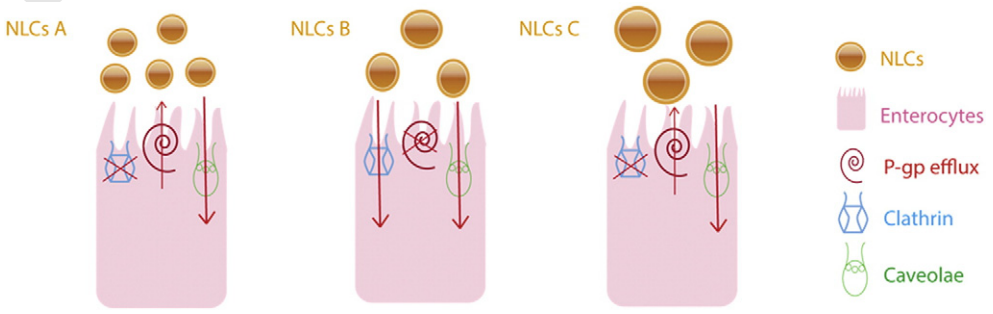

Fig. 7. Scheme of the transport mechanisms used by the different NLC formulations.

References

[1] A. Dahan, A. Hoffman, The effect of different lipid based formulations on the oral absorption of lipophilic drugs: the ability of in vitro lipolysis and consecutive ex vivo intestinal permeability data to predict in vivo bioavailability in rats, Eur. J. Pharm. Biopharm. 67 (2007) 96–105.

[2] E.M. Merisko-Liversidge, G.G. Liversidge, Drug nanoparticles: formulating poorly water-soluble compounds, Toxicol. Pathol. 36 (2008) 43–48.

[3] C.M. O'Driscoll, B.T. Griffin, Biopharmaceutical challenges associated with drugs with low aqueous solubility—the potential impact of lipid-based formulations, Adv. Drug Deliv. Rev. 60 (2008) 617–624.

[4] Y. Kawabata, K. Wada, M. Nakatani, S. Yamada, S. Onoue, Formulation design for poorly water-soluble drugs based on biopharmaceutics classification system: basic approaches and practical applications, Int. J. Pharm. 420 (2011) 1–10.

[5] E. Merisko-Liversidge, G.G. Liversidge, Nanosizing for oral and parenteral drug delivery: a perspective on formulating poorly-water soluble compounds using wet media milling technology, Adv. Drug Deliv. Rev. 63 (2011) 427–440.

[6] O.C. Farokhzad, R. Langer, Impact of nanotechnology on drug delivery, ACS Nano 3 (2009) 16–20.

[7] J. Shi, A.R. Votruba, O.C. Farokhzad, R. Langer, Nanotechnology in drug delivery and tissue engineering: from discovery to applications, Nano Lett. 10 (2010) 3223–3230.

[8] P. Couvreur, Nanoparticles in drug delivery: Past, present and future, Adv. Drug Deliv. Rev. (in press).

[9] C.E. Mora-Huertas, H. Fessi, A. Elaissari, Polymer-based nanocapsules for drug delivery, Int. J. Pharm. 385 (2010) 113–142.

[10] A. Elgart, I. Cherniakov, Y. Aldouby, A.J. Domb, A. Hoffman, Lipospheres and pro-nano lipospheres for delivery of poorly water soluble compounds, Chem. Phys. Lipids 165 (2012) 438–453.

[11] N.T. Huynh, C. Passirani, P. Saulnier, J.P. Benoit, Lipid nanocapsules: a new platform for nanomedicine, Int. J. Pharm. 379 (2009) 201–209.

[12] M. Muchow, P. Maincent, R.H. Muller, Lipid nanoparticles with a solid matrix (SLN, NLC, LDC) for oral drug delivery, Drug Dev. Ind. Pharm. 34 (2008) 1394–1405.

[13] G. Gaucher, P. Satturwar, M.-C. Jones, A. Furtos, J.-C. Leroux, Polymeric micelles for oral drug delivery, Eur. J. Pharm. Biopharm. 76 (2010) 147–158.

[14] V.P. Sant, D. Smith, J.-C. Leroux, Enhancement of oral bioavailability of poorly water-soluble drugs by poly(ethylene glycol)-block-poly(alkyl acrylate-co-methacrylic acid) self-assemblies, J. Control. Release 104 (2005) 289–300.

[15] X. Pu, J. Sun, M. Li, Z. He, Formulation of nanosuspensions as a new approach for the delivery of poorly soluble drugs, Curr. Nanosci. 5 (2009) 417–427.

[16] R.H. Müller, K. Mäder, S. Gohla, Solid lipid nanoparticles (SLN) for controlled drug delivery — a review of the state of the art, Eur. J. Pharm. Biopharm. 50 (2000) 161–177.

[17] R.H. Müller, M. Radtke, S.A. Wissing, Nanostructured lipid matrices for improved microencapsulation of drugs, Int. J. Pharm. 242 (2002) 121–128.

[18] M. Muchow, P. Maincent, R. Muller, Lipid nanoparticles with a solid matrix (SLN, NLC, LDC) for oral drug delivery, Drug Dev. Ind. Pharm. 34 (2008) 1394–1405.

[19] J. Rejman, V. Oberle, I.S. Zuhorn, D. Hoekstra, Size-dependent internalization of particles via the pathways of clathrin- and caveolae-mediated endocytosis, Biochem. J. 377 (2004) 159–169.

[20] O. Harush-Frenkel, E. Rozentur, S. Benita, Y. Altschuler, Surface charge of nanoparticles determines their endocytic and transcytotic pathway in polarized MDCK cells, Biomacromolecules 9 (2008) 435–443.

[21] M. Gaumet, R. Gurny, F. Delie, Interaction of biodegradable nanoparticles with intestinal cells: the effect of surface hydrophilicity, Int. J. Pharm. 390 (2010) 45–52.

[22] H. Hillaireau, P. Couvreur, Nanocarriers' entry into the cell: relevance to drug delivery, Cell. Mol. Life Sci. 66 (2009) 2873–2896.

[23] F. Mathot, A. des Rieux, A. Ariën, Y.J. Schneider, M. Brewster, V. Préat, Transport mechanisms of mmePEG750P(CL-co-TMC) polymeric micelles across the intestinal barrier, J. Control. Release 124 (2007) 134–143.

[24] E. Roger, F. Lagarce, E. Garcion, J.P. Benoit, Lipid nanocarriers improve paclitaxel transport throughout human intestinal epithelial cells by using vesicle-mediated transcytosis, J. Control. Release 140 (2009) 174–181.

[25] I. Behrens, A.I. Pena, M.J. Alonso, T. Kissel, Comparative uptake studies of bioadhesive and non-bioadhesive nanoparticles in human intestinal cell lines and rats: the effect of mucus on particle adsorption and transport, Pharm. Res. 19 (2002) 1185–1193.

[26] A. des Rieux, E.G.E. Ragnarsson, E. Gullberg, V. Préat, Y.-J. Schneider, P. Artursson, Transport of nanoparticles across an in vitro model of the human intestinal follicle associated epithelium, Eur. J. Pharm. Sci. 25 (2005) 455–465.

[27] A. des Rieux, V. Fievez, I. Théate, J. Mast, V. Préat, Y.-J. Schneider, An improved in vitro model of human intestinal follicle-associated epithelium to study nanoparticle transport by M cells, Eur. J. Pharm. Sci. 30 (2007) 380–391.

[28] R. Müller, K. Mäder, S. Gohla, Solid lipid nanoparticles (SLN) for controlled drug delivery — a review of the state of the art, Eur. J. Pharm. Biopharm. 50 (2000) 161–177.

[29] R.H. Müller, D. Rühl, M. Lück, B.R. Paulke, Influence of fluorescent labelling of polystyrene particles on phagocytic uptake, surface hydrophobicity, and plasma protein adsorption, Pharm. Res. 14 (1997) 18–24.

[30] V. Albert, P. Modamio, C.F. Lastra, E.L. Mariño, Determination of saquinavir and ritonavir in human plasma by reversed-phase high-performance liquid chromatography and the analytical error function, J. Pharm. Biomed. Anal. 36 (2004) 835–840.

[31] M. Rescigno, M. Urbano, B. Valzasina, M. Francolini, G. Rotta, R. Bonasio, F. Granucci, J.-P. Kraehenbuhl, P. Ricciardi-Castagnoli, Dendritic cells express tight junction proteins and penetrate gut epithelial monolayers to sample bacteria, Nat. Immunol. 2 (2001) 361–367.

[32] A. des Rieux, V. Fievez, M. Momtaz, C. Detrembleur, M. Alonso-Sande, J. Van Gelder, A. Cauvin, Y.-J. Schneider, V. Préat, Helodermin-loaded nanoparticles: characterization and transport across an in vitro model of the follicle-associated epithelium, J. Control. Release 118 (2007) 294–302.

[33] P.B. Memvanga, V. Préat, Formulation design and in vivo antimalarial evaluation of lipid-based drug delivery systems for oral delivery of β-arteether, Eur. J. Pharm. Biopharm. 82 (2012) 112–119.

[34] E. Gullberg, M. Leonard, J. Karlsson, A.M. Hopkins, D. Brayden, A.W. Baird, P. Artursson, Expression of specific markers and particle transport in a new human intestinal M-cell model, Biochem. Biophys. Res. Commun. 279 (2000) 808–813.

[35] Z. Zhang, F. Gao, H. Bu, J. Xiao, Y. Li, Solid lipid nanoparticles loading candesartan cilexetil enhance oral bioavailability: in vitro characteristics and absorption mechanism in rats, Nanomedicine 8 (2012) 740–747.

[36] S. Matveev, X. Li, W. Everson, E.J. Smart, The role of caveolae and caveolin in vesicle-dependent and vesicle-independent trafficking, Adv. Drug Deliv. Rev. 49 (2001) 237–250.

[37] S.K. Rodal, G. Skretting, O. Garred, F. Vilhardt, B. van Deurs, K. Sandvig, Extraction of cholesterol with methyl-beta-cyclodextrin perturbs formation of clathrin-coated endocytic vesicles, Mol. Biol. Cell 10 (1999) 961–974.

[38] B.J. Aungst, P-glycoprotein, secretory transport, and other barriers to the oral delivery of anti-HIV drugs, Adv. Drug Deliv. Rev. 39 (1999) 105–116.

[39] S.J. Mouly, M.F. Paine, P.B. Watkins, Contributions of CYP3A4, P-glycoprotein, and serum protein binding to the intestinal first-pass extraction of saquinavir, J. Pharmacol. Exp. Ther. 308 (2004) 941–948.

[40] E. Roger, F. Lagarce, E. Garcion, J.P. Benoit, Reciprocal competition between lipid nanocapsules and P-gp for paclitaxel transport across Caco-2 cells, Eur. J. Pharm. Sci. 40 (2010) 422–429.

[41] I. Rivolta, A. Panariti, B. Lettiero, S. Sesana, P. Gasco, M.R. Gasco, M. Masserini, G. Miserocchi, Cellular uptake of coumarin-6 as a model drug loaded in solid lipid nanoparticles, J. Physiol. Pharmacol. 62 (2011) 45–53.

[42] A. del Pozo-Rodríguez, D. Delgado, M.Á. Solinís, J.L. Pedraz, E. Echevarría, J.M. Rodríguez, A.R. Gascón, Solid lipid nanoparticles as potential tools for gene therapy: in vivo protein expression after intravenous administration, Int. J. Pharm. 385 (2010) 157–162.

[43] J. Weiss, J. Burhenne, K.D. Riedel, W.E. Haefeli, Poor solubility limiting significance of in-vitro studies with HIV protease inhibitors, AIDS 16 (2002) 674–676.

[44] F. Föger, K. Kafedjiiski, H. Hoyer, B. Loretz, A. Bernkop-Schnürch, Enhanced transport of P-glycoprotein substrate saquinavir in presence of thiolated chitosan, J. Drug Target. 15 (2007) 132–139.

[45] S.M. Pathak, P. Musmade, S. Dengle, A. Karthik, K. Bhat, N. Udupa, Enhanced oral absorption of saquinavir with methyl-beta-cyclodextrin—preparation and in vitro and in vivo evaluation, Eur. J. Pharm. Sci. 41 (2010) 440–451.

[46] T.H. Ermak, P.J. Giannasca, Microparticle targeting to M cells, Adv. Drug Deliv. Rev. 34 (1998) 261–283.

[47] B. D'Souza, T. Bhowmik, R. Shashidharamurthy, C. Oettinger, P. Selvaraj, M. D'Souza, Oral microparticulate vaccine for melanoma using M-cell targeting, J. Drug Target. 20 (2011) 166–173.

[48] L.M. Ensign, R. Cone, J. Hanes, Oral drug delivery with polymeric nanoparticles: the gastrointestinal mucus barriers, Adv. Drug Deliv. Rev. 64 (2012) 557–570.

[49] M. Liang, I.C. Lin, M.R. Whittaker, R.F. Minchin, M.J. Monteiro, I. Toth, Cellular uptake of densely packed polymer coatings on gold nanoparticles, ACS Nano 4 (2009) 403–413.

[50] H. Tomoda, Y. Kishimoto, Y.C. Lee, Temperature effect on endocytosis and exocytosis by rabbit alveolar macrophages, J. Biol. Chem. 264 (1989) 15445–15450.

[51] S. Mayor, R.E. Pagano, Pathways of clathrin-independent endocytosis, Nat. Rev. Mol. Cell Biol. 8 (2007) 603–612.

[52] Z.-J. Cheng, R.D. Singh, D.K. Sharma, E.L. Holicky, K. Hanada, D.L. Marks, R.E. Pagano, Distinct mechanisms of clathrin-independent endocytosis have unique sphingolipid requirements, Mol. Biol. Cell 17 (2006) 3197–3210.

[53] G. Sahay, D.Y. Alakhova, A.V. Kabanov, Endocytosis of nanomedicines, J. Control. Release 145 (2010) 182–195.

[54] I.R. Nabi, P.U. Le, Caveolae/raft-dependent endocytosis, J. Cell Biol. 161 (2003) 673–677.

[55] M. Kirkham, R.G. Parton, Clathrin-independent endocytosis: new insights into caveolae and non-caveolar lipid raft carriers, Biochim. Biophys. Acta 1745 (2005) 273–286.

[56] R.G. Parton, A.A. Richards, Lipid rafts and caveolae as portals for endocytosis: new insights and common mechanisms, Traffic 4 (2003) 724–738.

[57] A. Paillard, F. Hindré, C. Vignes-Colombeix, J.P. Benoit, E. Garcion, The importance of endo-lysosomal escape with lipid nanocapsules for drug subcellular bioavailability, Biomaterials 31 (2010) 7542–7554.

[58] A. del Pozo-Rodríguez, S. Pujals, D. Delgado, M.A. Solinís, A.R. Gascón, E. Giralt, J.L. Pedraz, A proline-rich peptide improves cell transfection of solid lipid nanoparticle-based non-viral vectors, J. Control. Release 133 (2009) 52–59.

[59] M. Simionescu, D. Popov, A. Sima, Endothelial transcytosis in health and disease, Cell Tissue Res. 335 (2009) 27–40.

[60] K. Yunomae, H. Arima, F. Hirayama, K. Uekama, Involvement of cholesterol in the inhibitory effect of dimethyl-β-cyclodextrin on P-glycoprotein and MRP2 function in Caco-2 cells, FEBS Lett. 536 (2003) 225–231.

[61] A. Garrigues, A.E. Escargueil, S. Orlowski, The multidrug transporter, P-glycoprotein, actively mediates cholesterol redistribution in the cell membrane, Proc. Natl. Acad. Sci. U. S. A. 99 (2002) 10347–10352.
[62] S. Barakat, M. Demeule, A. Pilorget, A. Régina, D. Gingras, L.G. Baggetto, R. Béliveau, Modulation of p-glycoprotein function by caveolin-1 phosphorylation, J. Neurochem. 101 (2007) 1–8.
[63] R. Nieto Montesinos, A. Béduneau, Y. Pellequer, A. Lamprecht, Delivery of P-glycoprotein substrates using chemosensitizers and nanotechnology for selective and efficient therapeutic outcomes, J. Control. Release 161 (2012) 50–61.

Please cite this article as: A. Beloqui, et al., Mechanism of transport of saquinavir-loaded nanostructured lipid carriers across the intestinal barrier, J. Control. Release (2012), http://dx.doi.org/10.1016/j.jconrel.2012.12.021